Journal of Solid State Chemistry **148,** 455–463 (1999)
Article ID jssc.1999.8479, available online at http://www.idealibrary.com on IDEAL®

Structure Refinement and Magnetic Properties of C–$Fe(PO_3)_3$ Studied by Neutron Diffraction and Mössbauer Techniques

L. K. Elbouaanani, B. Malaman, and R. Gérardin

Laboratoire de Chimie du Solide Minéral, Université Henri Poincaré-Nancy I, associé au CNRS (UMR 7555), B.P. 239, 54506 Vandoeuvre les Nancy Cedex, France

Received May 14, 1999; in revised form July 28, 1999; accepted August 10, 1999

C–$Fe(PO_3)_3$ has been synthesized using H_3PO_4 and $Fe(NO_3)_3 \cdot 9H_2O$ as starting compounds. Single crystals were grown under vacuum with a trace of $FeCl_2$. $Fe(PO_3)_3$ crystallizes in the monoclinic space group *Cc*, with $a = 13.148(4)$ Å, $b = 19.076(2)$ Å, $c = 9.410(3)$ Å, $\beta = 127.00(2)^\circ$, and $Z = 12$. Its structure has been determined through direct methods and difference Fourier synthesis and has been refined to $R = 0.0405$ ($R_W = 0.047$). $Fe(PO_3)_3$ belongs to a series of isotypic $M(PO_3)_3$ trimetaphosphates (M = Al, V, Sc, In, Ti, Mo, Rh, Cr) which are characterized by a tridimensional network of isolated MO_6 octahedra connected through PO_4 tetrahedra. $Fe(PO_3)_3$ is antiferromagnetic below $T_N = 10$ K. The magnetic structure has been determinated by means of powder neutron diffraction: each iron atom is linked to six iron nearest neighbors of opposite spin, through six single Fe–O–P–O–Fe superexchange pathways. The moment direction lies in the (010) plane, making an angle of $\sim 32^\circ$ with the *a* axis ($\mu \sim 4.4\ \mu_B$). Mössbauer spectra are fitted with two doublets and three sextuplets in the paramagnetic and the antiferromagnetic states, respectively. Their rather high isomer shifts are explained by the inductive effect.

INTRODUCTION

Monoclinic C-type $Fe(PO_3)_3$ compound is one of six polymorphic modifications reported in the literature for this phosphate (1, 2). According to Durif (3), this compound is a member of a series of isotypic trimetaphosphates $M(PO_3)_3$ with M = Al (4), V (5), Sc (6), In (7), Ti (8), Mo (9), Rh (10), Cr (11); up to now, only characterization from powder data was available. On the other hand, $Fe(PO_3)_3$ exhibits an antiferromagnetic behavior below $T_N = 10$ K (12). In these compounds, M atoms are isolated from each other and are only connected by PO_4 groups yielding, in the case of $Fe(PO_3)_3$, to Fe–O–P–O–Fe super-exchange as only magnetic interactions.

In the course of an investigation of mixed-valent iron phosphates (13) and silico-phosphates (14), we decide to reinvestigate the physical properties of this compound. In this paper we report on its structural and magnetic properties by means of single-crystal X-ray diffraction, bulk magnetization, powder neutron diffraction, and Mössbauer spectroscopy measurements.

EXPERIMENTAL

$Fe(PO_3)_3$ has been prepared by evaporation of a solution of $Fe(NO_3)_3 \cdot 9H_2O$ and H_3PO_4 with the ratio Fe : P = 1 : 3 and annealing at 400°C under nitrogen, then at 900°C under oxygen for 24 h. Single crystals were grown by long annealing (1 month), in sealed silica tubes, within a gold crucible, under vacuum, at 900°C, with traces of $FeCl_2$ as mineralizer agent. A single crystal (~ 100 μm) was selected for the structure determination. The data were collected on a Nonius CAD 4 automatic diffractometer at the Service Commun de Diffractométrie de l'Université Henri Poincaré-Nancy I.

Magnetic measurements were performed (between 4.2 and 300 K) on a MANICS magneto-susceptometer in fields up to 1.6 T.

Neutron diffraction experiments were carried out at the Institut Laue Langevin, Grenoble. Several diffraction patterns were recorded with the one-dimensional curved multidetector D20 using a neutron wavelength of 2.410 Å, in the temperature range 300–2 K. The analysis of the patterns was performed by Rietveld profile refinements using the software Fullprof (15).

The Mössbauer data were collected with a constant acceleration spectrometer with 1024 channels. Isomer shifts are reported with respect to α-iron at room temperature. The Mössbauer effect data were analyzed by using least-squares minimization techniques (16) to evaluate the hyperfine spectral parameters.

CRYSTAL STRUCTURE

a. Structure Determination

The cell parameters (Table 1) were determined by least-squares refinements of the 2θ values of 25 independent reflections–antireflections, measured for $2\theta > 20^\circ$. The

0022-4596/99 $30.00

TABLE 1
Summary of Data Collection and Structure Refinement for $Fe(PO_3)_3$

Molar mass (g mol^{-1})	292.76
Crystal size (μm)	$\varphi \sim 100$
Symmetry	monoclinic
a (Å)	13.148(4)
b (Å)	19.076(2)
c (Å)	9.410(3)
β (°)	127.00(2)
V (Å^3)	1884.9
Z	12
ρ_{cal} (g cm^{-3})	3.10
ρ_{mes} (g cm^{-3})[a]	3.06(5)
Space group	Cc
Radiation	Mo$K\alpha$
Monochromator	graphite
Scanning	θ–2θ
Takeoff (°)	3.5°[a]
Record limits (°)	$\theta < 25$
Linear absorption coefficient μ (cm^{-1})	32.5
Recorded intensities	1961
Recorded intensities with $\sigma(I)/I < 0.33$	1037
$F(000)$	1716
Index ranges	$0 \leq h \leq 15$, $0 \leq k \leq 22$, $-11 \leq l \leq 8$
Number of parameters	155
Final R value	0.0405
Final R_w value	0.0472

[a] Pycnometer (decalin).

conditions for the data collection and refinement of the structure are listed in Table 1. Absorption was neglected ($\mu r \ll 1$). Atomic scattering factors for Fe^{3+}, P^0, and O^- were taken from Ref. (17). All computer programs used were taken from Ref. (18). The space group is Cc or $C2/c$; the structure determination has shown the first to be correct. The iron and phosphorus atomic positions were obtained using the direct methods procedure of the Shelx program (18). The oxygen atomic positions were determined, step by step, by difference Fourier synthesis. Final refinement with individual and isotropic temperature factors leads to the residual $R = 0.0405$ ($R_w = 0.047$). The atomic parameters are listed in Table 2, and the main interatomic distances and angles are given in Table 3.

b. Description

The structure of $Fe(PO_3)_3$ is built up from isolated FeO_6 octahedra linked through infinite chains of PO_4 tetrahedra (Figs. 1–3).

There are three distinct FeO_6 octahedra which are very similar, and their geometry is almost regular (Table 3). The average value of the Fe–O distances (1.98 Å, Table 3) is comparable with those reported for other phosphates (e.g., II-$NaFeP_2O_7$, Fe–O = 1.99 Å (19); $KBaFe_2(PO_4)_3$, Fe1–O = 1.99 Å and Fe2–O = 2.01 Å (20)).

FeO_6 octahedra are aligned along the [010] direction (Fig. 2). Each FeO_6 group is bridged to six FeO_6 octahedra by six PO_4 tetrahedra, the Fe–Fe distances varying from 5.3 to 5.82 Å (see Fig. 1, see also Fig. 9).

The phosphorus atoms P1, P6, and P7 are linked to each others via P1–O1–P7–O7–P6–O13–P1 creating infinite chains of tetrahedra PO_4 (three-membered). In the same way P2, P5, P8, P3, P4, and P9 are linked via P2–O10–P5–O15–P8–O16–P3–O25–P4–O26–P9–O17–P2 forming an infinite chain (six-membered) isolated from the former. Both chains run along the c axis (Fig. 3). The smallest and largest angles P–O–P are 137(1)° and 149(2)°, respectively. In each chain, the diphosphate groups are

TABLE 2
Fractional Atomic Coordinates and Thermal Agitation Factors

Atom	x	y	z	B (Å^2)
Fe(1)[a]	0.8439	0.0784(2)	0.0717	0.0045(7)
Fe(2)	0.8250(4)	0.2443(2)	− 0.4623(5)	0.0057(11)
Fe(3)	0.3477(5)	0.0890(2)	− 0.4260(7)	0.0053(8)
P(1)	0.7110(8)	− 0.0306(3)	− 0.2506(10)	0.0065(15)
P(2)	0.6990(8)	0.3017(3)	− 0.2756(10)	0.0071(16)
P(3)	0.6946(8)	0.3633(4)	0.2269(10)	0.0064(15)
P(4)	0.1115(7)	0.0209(3)	− 0.1523(9)	0.0052(13)
P(5)	0.5976(7)	0.1865(3)	− 0.1744(10)	0.0030(14)
P(6)	0.4905(7)	0.0263(3)	− 0.5923(9)	0.0039(14)
P(7)	0.5698(8)	0.1459(4)	− 0.7213(11)	0.0085(16)
P(8)	0.4764(8)	0.3048(3)	− 0.1240(10)	0.0075(16)
P(9)	0.9772(8)	0.1354(3)	− 0.1162(10)	0.0030(14)
O(1)	0.6130(20)	0.0930(10)	0.1980(26)	0.0146(43)
O(2)	0.6830(15)	0.1318(7)	0.9562(19)	0.0041(31)
O(3)	0.8773(16)	0.1078(8)	0.9007(22)	0.0068(36)
O(4)	0.6865(15)	0.1739(8)	0.4364(21)	0.0014(34)
O(5)	0.2984(14)	0.2092(8)	0.2005(18)	0.0011(30)
O(6)	0.3987(16)	0.0346(8)	0.4478(20)	0.0077(36)
O(7)	0.4992(16)	0.0982(8)	0.3318(20)	0.0026(35)
O(8)	0.8199(15)	0.0547(8)	0.2512(19)	0.0012(35)
O(9)	0.4753(16)	0.1919(8)	0.1384(21)	0.0081(40)
O(10)	0.6794(15)	0.2301(8)	0.7877(19)	0.0094(35)
O(11)	0.3016(15)	0.1357(8)	0.7137(20)	0.0044(31)
O(12)	0.2125(14)	0.0230(8)	0.5036(19)	0.0053(32)
O(13)	0.6265(18)	0.0248(9)	0.5971(21)	0.0089(40)
O(14)	0.4782(15)	0.1617(8)	0.6517(22)	0.0074(34)
O(15)	0.5635(15)	0.2413(7)	0.9225(20)	0.0023(30)
O(16)	0.0612(14)	0.1452(7)	0.5355(19)	0.0048(32)
O(17)	0.0615(14)	0.1896(7)	0.0424(18)	0.0038(31)
O(18)	0.2244(15)	0.1430(7)	0.3486(19)	0.0066(31)
O(19)	0.4738(15)	0.0327(7)	0.7892(19)	0.0001(30)
O(20)	0.8645(17)	0.2121(9)	0.3740(22)	0.0120(39)
O(21)	0.7444(17)	0.0015(9)	0.9199(22)	0.0094(42)
O(22)	0.9453(15)	0.1649(7)	0.2116(19)	0.0053(33)
O(23)	0.9365(13)	0.1671(7)	0.7139(18)	0.0035(31)
O(24)	0.1999(15)	0.1879(7)	0.8497(20)	0.0065(30)
O(25)	0.1770(14)	0.0614(8)	0.7731(18)	0.0042(31)
O(26)	0.0755(15)	0.0776(7)	0.9318(19)	0.0003(30)
O(27)	− 0.0033(16)	0.0160(9)	0.1928(21)	0.0115(35)

[a] Atom chosen for fixing the origin.

TABLE 3
Main Interatomic Distances (Å) and Angles (°)

Fe(1)–O(21)	1.91(2)	Fe(2)–O(5)	1.97(2)	Fe(3)–O(12)	1.94(2)
–O(8)	1.95(2)	–O(4)	1.99(2)	–O(11)	1.96(2)
–O(2)	1.98(2)	–O(20)	1.99(3)	–O(6)	1.97(2)
–O(3)	1.99(2)	–O(24)	2.00(1)	–O(14)	1.97(2)
–O(27)	2.00(2)	–O(9)	2.01(2)	–O(19)	1.99(1)
–O(22)	2.03(1)	–O(23)	2.04(1)	–O(18)	2.01(1)
P(1)–O(8)	1.49(2)	P(2)–O(18)	1.46(2)	P(3)–O(24)	1.48(2)
–O(21)	1.52(2)	–O(5)	1.47(2)	–O(11)	1.48(3)
–O(13)	1.58(2)	–O(10)	1.57(2)	–O(25)	1.56(2)
–O(1)	1.60(2)	–O(17)	1.58(1)	–O(16)	1.60(1)
P(4)–O(27)	1.50(1)	P(5)–O(2)	1.48(1)	P(6)–O(6)	1.47(3)
–O(12)	1.51(1)	–O(14)	1.51(1)	–O(19)	1.50(2)
–O(26)	1.57(2)	–O(10)	1.56(2)	–O(7)	1.58(2)
–O(25)	1.60(2)	–O(15)	1.62(2)	–O(13)	1.60(1)
P(7)–O(9)	1.44(1)	P(8)–O(22)	1.46(2)	P(9)–O(23)	1.48(2)
–O(4)	1.45(1)	–O(20)	1.50(3)	–O(3)	1.51(3)
–O(1)	1.56(3)	–O(15)	1.54(2)	–O(26)	1.55(2)
–O(7)	1.58(2)	–O(16)	1.55(1)	–O(17)	1.59(1)
O(21)–P(1)–O(8)	116(1)	O(5)–P(2)–O(18)	115(1)	O(11)–P(3)–O(24)	118(1)
O(13)–O(8)	111(1)	O(10)–O(18)	110(1)	O(25)–O(24)	110(1)
–O(21)	107(1)	–O(5)	107(1)	–O(11)	109(1)
O(1)–O(8)	112(1)	O(17)–O(18)	111(1)	O(16)–O(24)	108(1)
–O(21)	107(1)	–O(5)	113(1)	–O(11)	111(1)
–O(13)	103(1)	–O(10)	99.2(9)	–O(25)	99.3(8)
O(12)–P(4)–O(27)	117.9(9)	O(14)–P(5)–O(2)	117.0(8)	O(19)–P(6)–O(6)	119(1)
O(26)–O(27)	112(1)	O(10)–O(2)	106(1)	O(7)–O(6)	108(1)
–O(12)	104(1)	–O(14)	109(1)	–O(19)	109(1)
O(25)–O(27)	107(1)	O(15)–O(2)	108(1)	O(13)–O(6)	105(1)
–O(12)	108(1)	–O(14)	111(1)	–O(19)	112(1)
–O(26)	107(1)	–O(10)	104(1)	–O(7)	100.6(9)
O(4)–P(7)–O(9)	121(1)	O(20)–P(8)–O(22)	115(1)	O(3)–P(9)–O(23)	119(1)
O(1)–O(9)	108(1)	O(15)–O(22)	108(2)	O(26)–O(23)	108(1)
–O(4)	105(1)	–O(20)	113(1)	–O(3)	110(1)
O(7)–O(9)	107(1)	O(16)–O(22)	111(1)	O(17)–O(23)	110.2(9)
–O(4)	110(1)	–O(20)	106(1)	–O(3)	107(1)
–O(1)	104(1)	–O(15)	103.2(8)	–O(26)	101.5(8)

condensed in both nearly staggered and eclipsed conformations, in the ratio two staggered for one eclipsed.

Bearing these observations in mind, each PO_4 tetrahedron shares corners with two FeO_6 and two PO_4 polyhedra

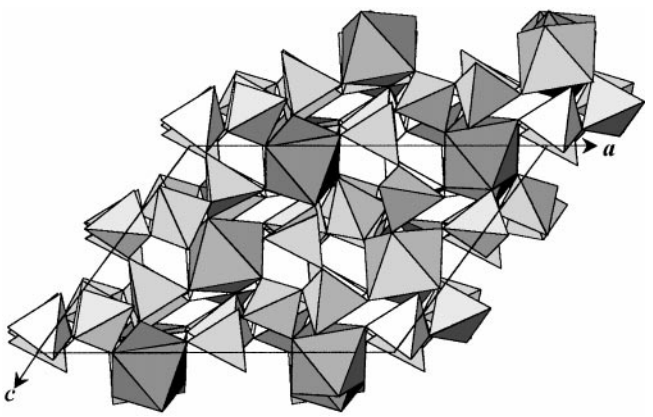

FIG. 1. Projection of the structure of $Fe(PO_3)_3$ along the *b* axis.

leading to two sets of P–O distances. The first ones involve P–O–Fe bonds with a mean d_{P-O} value of ~ 1.48 Å while the second ones correspond to P–O–P bridges with a classical mean d_{P-O} value of ~ 1.58 Å (13). This yields an average P–O distance of 1.53 Å (Table 3), which is comparable to the 1.536 Å value given by Corbridge (21). Furthermore, as shown in Table 3, one observes that shorter *d*(P–O) bonds involve wider O–P–O angles: (Fe)–O–P–O–(Fe) > (Fe)–O–P–O–(P) > (P)–O–P–O–(P). This point has been largely discussed in Ref. (13).

It is noteworthy that similar features have been encountered in all the other C-form polyphosphates (4–11).

MAGNETIC STUDY

a. Susceptibility Measurements

The thermal variations of χ and $1/\chi$ are shown in Fig. 4. There is a paramagnetic–antiferromagnetic transition at

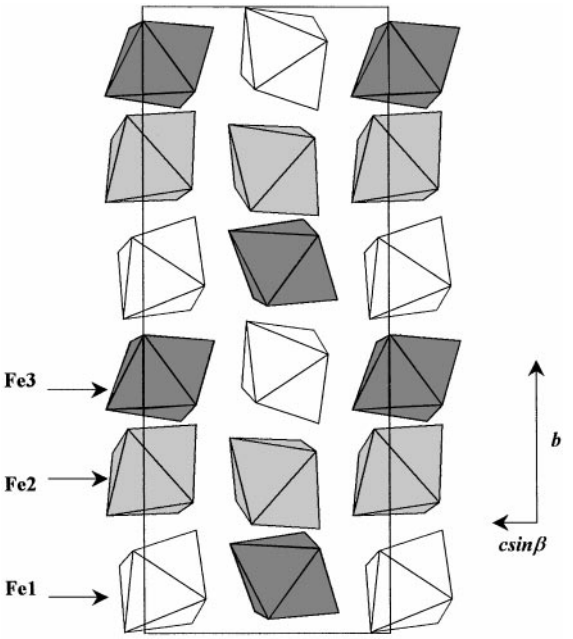

FIG. 2. Projection of the FeO6 octahedra along the *a* axis.

$T_N = 10$ K in agreement with the previously reported data (12). In the paramagnetic state, immediately above T_N, the Curie–Weiss law is obeyed and the apparent effective magnetic moment is $\mu_{eff} \sim 6.1\ \mu_B$, close to the value expected for Fe^{3+} in the high-spin ground state. The extrapolate Curie temperature is negative: $\theta_p = -16$ K.

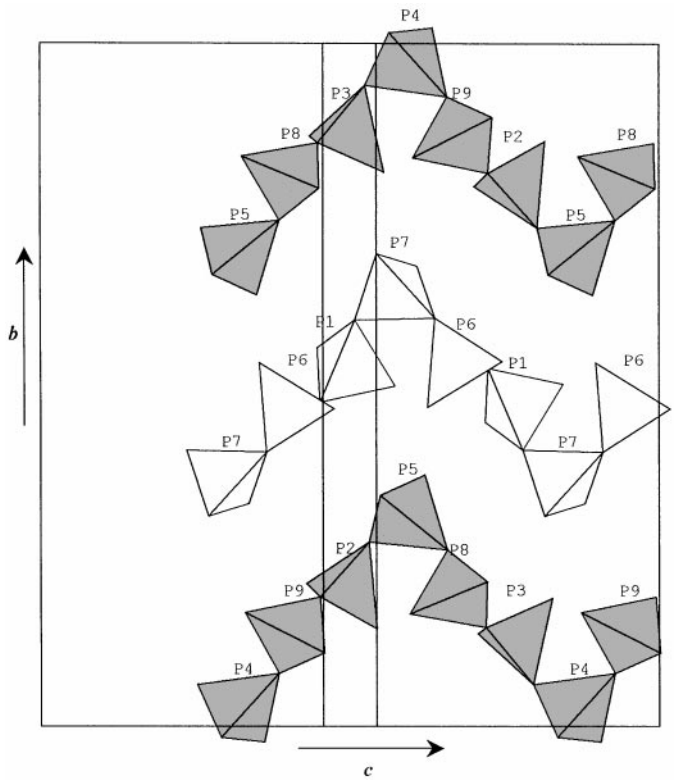

FIG. 3. Projection on the (100) plane, the polyphosphate chains undulating along the *c* axis.

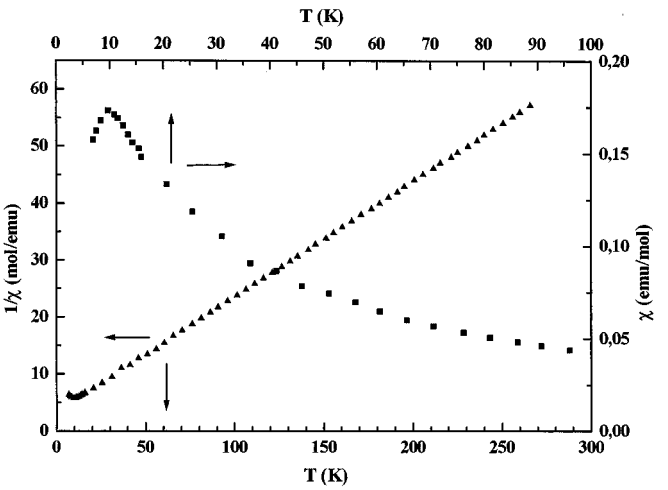

FIG. 4. Thermal variation of the direct and reciprocal susceptibility.

b. Neutron Diffraction Study

Neutron diffraction patterns recorded at 100 and 2 K are shown in Fig. 5. At 100 K, the neutron diffraction pattern is characteristic of the only nuclear scattering. At 2 K, additional lines, characteristic of an antiferromagnetic ordering, appear. These magnetic reflections can be indexed on the basis of the crystal unit cell and obey the rules (hkl) with $h + k = 2n$ (i.e., the C-centered mode remains) and $(h0l)$ with $l = 2n + 1$ (i.e., forbidden by the *c* glide plane). It must be noted that some of the nuclear reflections have magnetic contributions to their intensities.

A model in agreement with the loss of the *c* glide plane was used to analyze the low-temperature neutron diffraction pattern. The final refinement is shown in Fig. 5. The low-angle region of the 100 and 2 K patterns are shown in Fig. 6; the magnetic reflections are labeled for the low temperature.

It should be noted that a full refinement is not possible due to the lack of experimental information as there are 125 variable parameters to determine from 49 independent neutron data (219 line observations, Fig. 5). Therefore, using the set of nuclear parameters defined during the single-crystal X-ray study (Table 2), only the scale factor, the lattice and halfwidth parameters, and the magnetic moment components, *constrained to be equal for the three independent iron sites*, were refined. The best fit to the data ($R_{NUC} = 2.86\%$; $R_{MAG} = 5.08\%$) gives $\mu_{Fe^{3+}} = 4.42(3)\ \mu_B$. The moment direction lies in the *ac* plane, making an angle of 32° with the *a* axis, almost coinciding with the $[10\bar{2}]$ direction. As shown

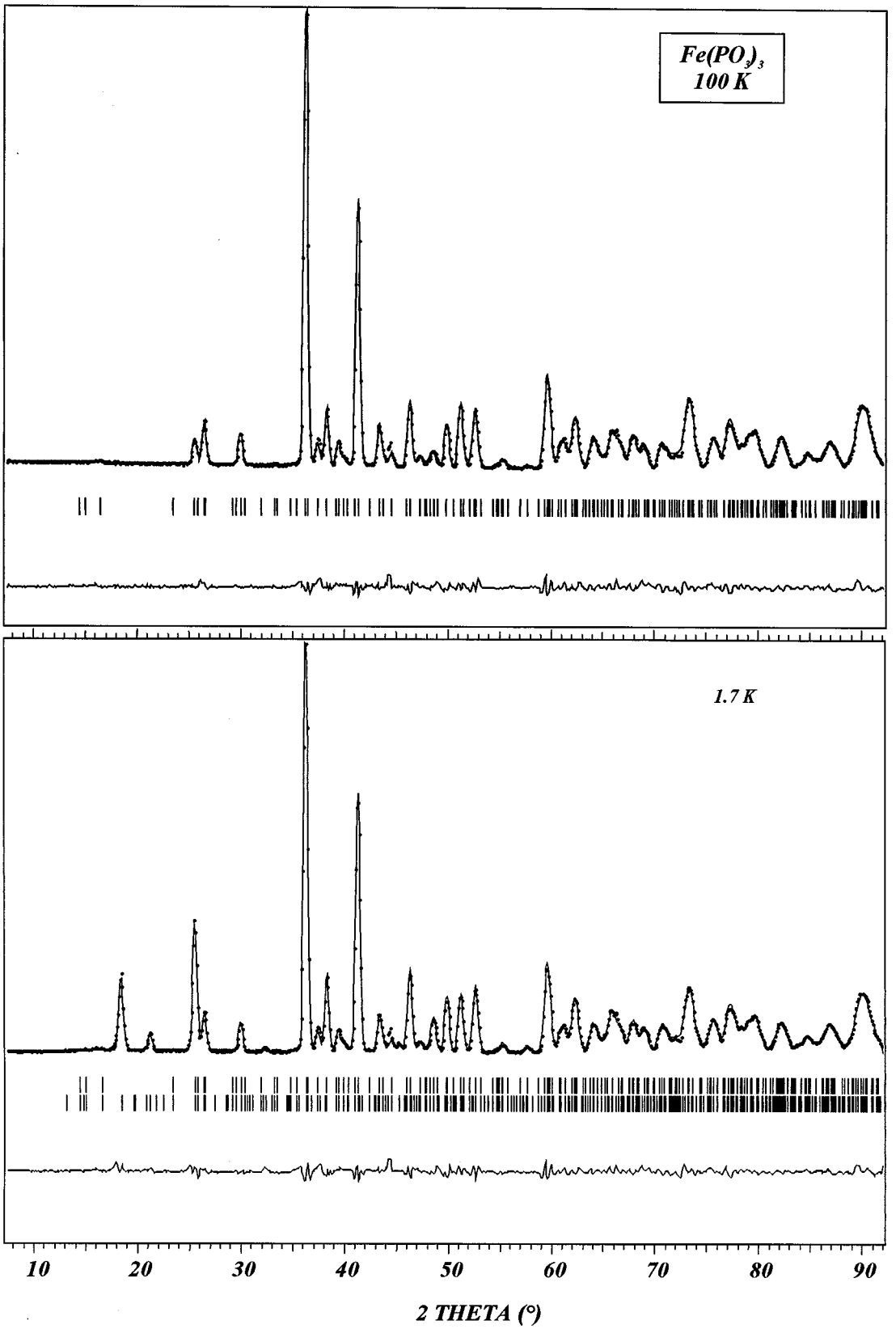

FIG. 5. Observed and calculated neutron pattern profiles of $Fe(PO_3)_3$ at 100 and 2 K.

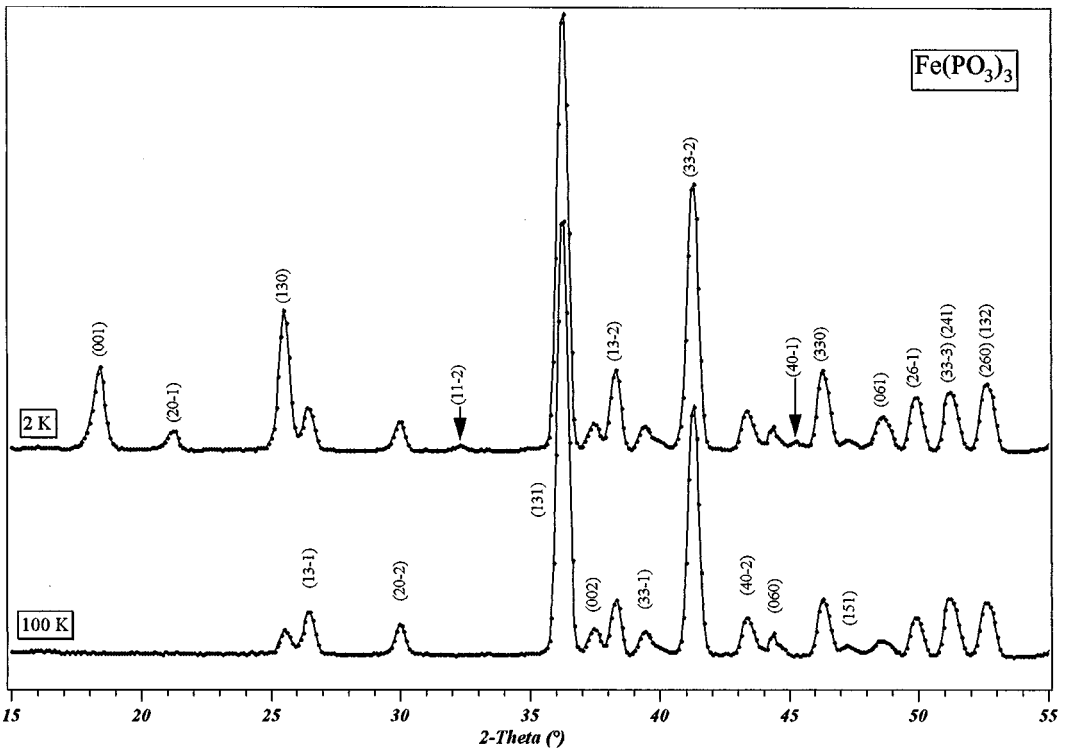

FIG. 6. Low angle of the neutron diffraction patterns at 2 and 100 K with magnetic peaks labeled ($\lambda = 2.410$ Å).

in Fig. 7, the iron atom network may be considered a deformed rock salt structure type where the iron magnetic moments formally replace the + and − charges: each iron atom is antiferromagnetically coupled with its six iron neighbors.

c. Mössbauer Spectrometry

Paramagnetic state. As shown on Fig. 8a, the spectra recorded at 295 and 11 K were fitted with two quadrupole doublets d1 and d2. The half-widths (Γ) and the isomer shifts (δ) were constrained to be equal. All the spectral parameters are listed in Table 4.

The isomer shift values are characteristic of high-spin Fe^{3+} in an octahedral oxygen environment (22). Their relatively high amplitudes probably originate from the rather high ionicity of the Fe–O bond: the high polarizing P atom withdraws electronic density on the P–O bond. This is in agreement with the previous structural information: the (P–O)–*Fe* distances are shorter than the (P–O)–*P* ones (Table 3). The room temperature values are closed to those observed for another phosphates (e.g., $\delta = 0.45$ for $NaFeP_2O_7$ (23) and $Na_3Fe_2(PO_4)_3$ (24)).

According to Brown and Altermatt (25), the oxidation state of the Fei cation V_{Fei} is related to s_{ij} (*the valence of the bond between the cation Fei and the anion* O_j) by the expression

$$V_{Fei} = \sum_{j=1}^{6} s_{ij} = \sum_{j=1}^{6} \exp[(r_0 - r_{ij})/B], \qquad [1]$$

where r_{ij} is the Fei–O_j bond length, r_0 and B are empirically determined parameters, $r_0 = 1.759$ for Fe^{3+}–O^{2-}, and $B = 0.37$ (25).

For the present compound, Eq. [1] yields to $V_{Fe1} = 3.350$, $V_{Fe2} = 3.133$, and $V_{Fe3} = 3.367$ for the three inequivalent iron atoms.

This result allows us to attribute the d1 and d2 quadrupole doublets to the Fe1, Fe2, and Fe3 atomic sites. Then, since the intensity ratio $I(d1)/I(d2) \sim 2$, we conclude that d2 corresponds to the Fe2 iron atom.

As shown in Fig. 2, the crystal structure of C–$Fe(PO_3)_3$ may be described as a stacking of (010) sheets made on FeO_6 octahedra. Hence, it is worth noting that Fe2 atoms are alone in their sheets, unlike the Fe1 and Fe3 atoms which occupy the same sheets in a 1 : 1 ratio.

Antiferromagnetic state. The transition to the magnetically ordered state is observed at ~10 K, in agreement with the previous bulk magnetization measurements. The internal magnetic hyperfine field (H) increases rapidly when the temperature decreases as shown in Fig. 8b. At 4.2 K we

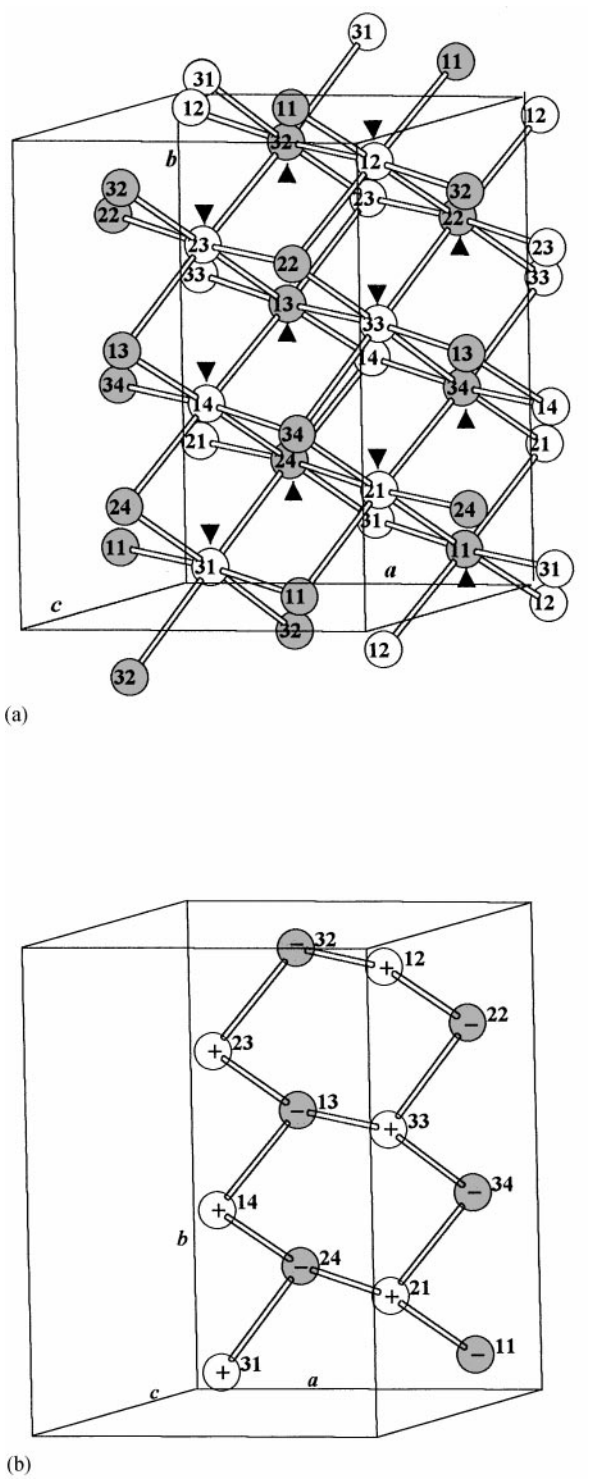

FIG. 7. Magnetic structure of $Fe(PO_3)_3$. The moments lie in the (010) plane. Only Fe atoms are shown and referenced as ij with $i = 1$ to 3 for the three irons' crystallographic sites; $j = 1$ to 2 corresponds to equivalent positions x, y, z and x, $-y$, $z + 1/2$, respectively, and 3 to 4 refer to the corresponding C–translation. (a) Each iron is antiferromagnetically coupled to six iron neighbors. Dark and light iron atoms are of opposite spin; ▼ corresponds to iron atoms in the unit cell (see (b)). (b) Only iron atoms in the unit cell are shown for clarity.

observe one sextet with large linewidths, whereas, at 6 K, the spectrum clearly displays three magnetic sextets, in fair agreement with the three independent iron sites of the non-centrosymetric space group *Cc* used in the X-ray diffraction study.

Each spectrum was fit with three magnetic sextets with equal isomer shifts. Since $\Delta_p(Fe1) = \Delta_p(Fe3)$ in the paramagnetic state, this property remains true in the ordered magnetic state. Consequently we have also constrained the corresponding quadrupole splittings Δ_0 to be equal. Bearing these preliminary remarks in mind, the spectra are fitted with a least-squares method program using the full Hamiltonian. The program gives the hyperfine field H, the quadrupole splitting Δ, the isomer shift δ, the asymmetry parameter η, and the polar angles θ, φ of the H direction in the EFG (*electric field gradient*) tensor principal-axes frame

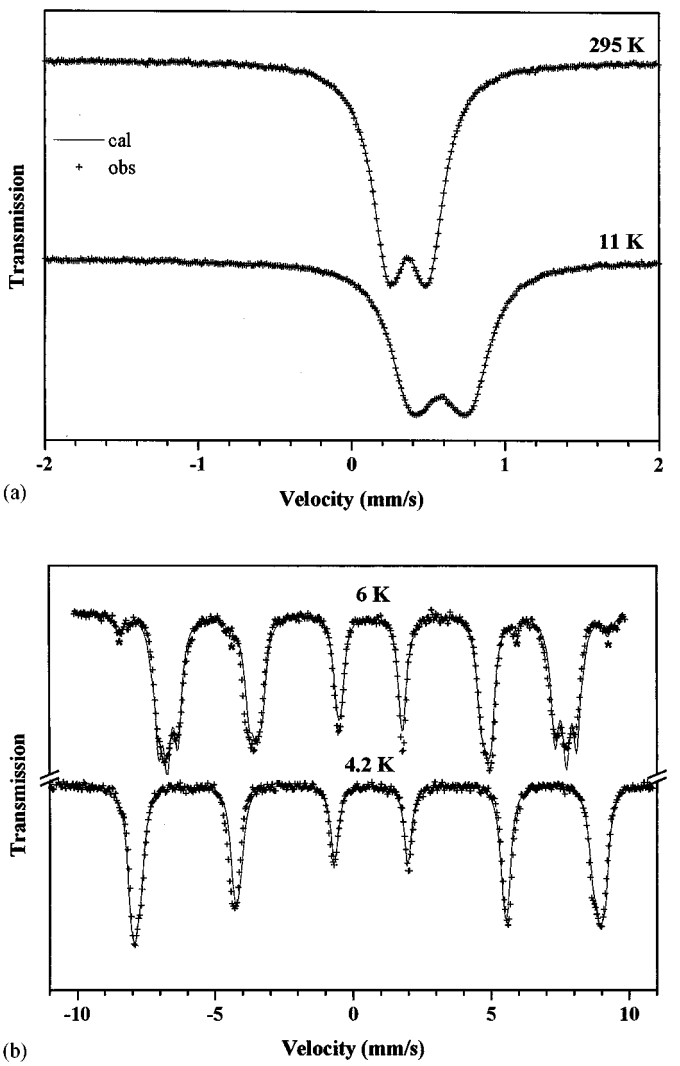

FIG. 8. (a) Paramagnetic Mössbauer spectra. (b) Ordered Mössbauer spectra (asterisks indicate $Fe_4(P_2O_7)_3$ as impurities).

TABLE 4
Mössbauer Spectral Parameters of $Fe(PO_3)_3$ in the Paramagnetic state

	Site 1 ($d1$)				Site 2 ($d2$)			
T (K)	δ	Δ_P	Γ	I (%)	δ	Δ_P	Γ	I (%)
298	0.443	0.390	0.31	65	0.443	0.213	0.31	35
70	0.578	0.420	0.33	66	0.578	0.205	0.33	34
11	0.576	0.425	0.29	64	0.576	0.189	0.29	36

Note. Γ, δ, Δ_P are given in mm s^{-1}, $\delta \pm 0.002$, $\Delta_P \pm 0.002$, $\Gamma \pm 0.01$, $I \pm 1$.

(16). Once the optimal solution is obtained, the Karyagin method (26) is applied to determine η, θ, and φ for each iron site.

At 4.2 K, the three magnetic hyperfine fields are refined to 510, 524, and 534 kOe. These values are quite similar and coherent with Fe^{3+} high-spin atoms nearly at the saturation state (H^{sat} (α-Fe_2O_3) = 550 kOe). Moreover, the best fit to the data allows us to assume that $\theta 1 = \theta 2 = \theta 3 = 90°$. In conjunction with the orientation of the magnetic moments of the iron atoms deduced from neutron data, one can conclude that V_{ZZ} is along [010] for each iron site.

Remark. It is worth noting that, in the case of the s3 site (Table 5), as η is relatively small (< 0.1), it is unreasonable to attribute a meaning to the φ angle values (27).

DISCUSSION

In C–$Fe(PO_3)_3$, the magnetic interactions arise from Fe–O–P–O–Fe superexchanges only (Fig. 9), which are characterized by the angle on phosphorus and by Fe–O bonds. As regards its strength, this superexchange is more effective the shorter the exchange pathway and the closer the angle at the phosphorus atom to the tetrahedral angle (28). The angles around the phosphorus are greater than

TABLE 5
Mössbauer Spectral Parameters of $Fe(PO_3)_3$ in the Antiferromagnetic State

T	Site	I (%)	Γ	δ	Δ_0	H	η	θ	φ
6 K[a]	s1	25	0.30	0.575	0.35	471	0.4	90	~0
	s2	34	0.35	0.575	0.18	450	0.8	90	90
	s3	31	0.35	0.575	0.35	425	~0.05	90	90–0
4.2 K	s1	33	0.32	0.585	0.35	534	0.4	90	~0
	s2	33	0.35	0.585	0.18	510	0.8	90	90
	s3	33	0.31	0.585	0.35	524	~0.05	90	0–90

Note. Γ, δ, Δ_0 are given in mm s^{-1}, the internal magnetic field in kOe (accurate ca. ± 1 kOe). $\Delta_0 = eQV_{zz}/2$.

[a] $Fe_4(P_2O_7)_3$ as impurities ($\sim 10\%$).

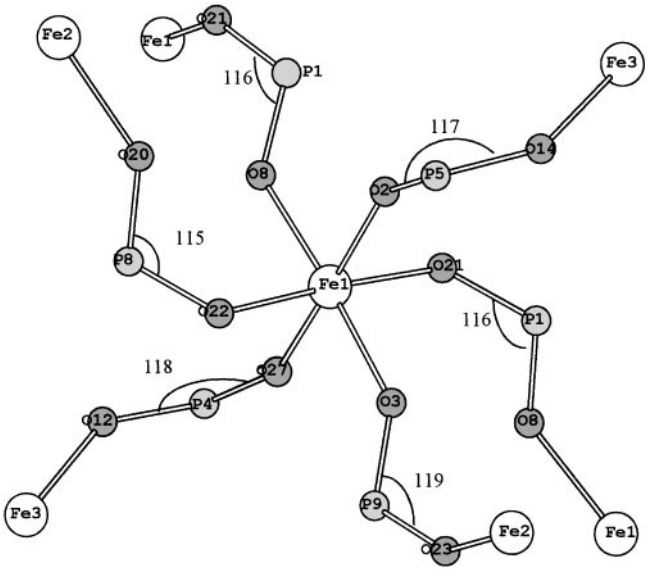

FIG. 9. The magnetic paths between Fe1 and its six neighbors.

TABLE 6
Magnetic Superexchange Pathways (See Fig. 8)

Interaction	Number total of bridges	Exchange type	Length of pathway (Å)	Angle on P (°)	Distance Fe..Fe (Å)
Fe1–O21–P1–O8–Fe1	1	AF	6.87	116	5.57
Fe1–O8–P1–O21–Fe1	1	AF	6.87	116	5.57
Fe1–O2–P5–O14–Fe3	1	AF	6.94	117	5.28
Fe1–O27–P4–O12–Fe3	1	AF	6.95	118	5.36
Fe1–O22–P8–O20–Fe2	1	AF	6.98	115	5.53
Fe1–O3–P9–O23–Fe2	1	AF	7.02	119	5.82
Average			6.94	117	5.52
Fe2–O4–P7–O9–Fe2	1	AF	6.89	121	5.32
Fe2–O9–P7–O4–Fe2	1	AF	6.89	121	5.32
Fe2–O20–P8–O22–Fe1	1	AF	6.98	115	5.53
Fe2–O23–P9–O3–Fe1	1	AF	7.02	119	5.82
Fe2–O24–P3–O11–Fe3	1	AF	6.92	118	5.82
Fe2–O5–P2–O18–Fe3	1	AF	6.91	115	5.55
Average			6.93	118	5.56
Fe3–O6–P6–O19–Fe3	1	AF	6.93	119	5.80
Fe3–O6–P6–O19–Fe3	1	AF	6.93	119	5.80
Fe3–O11–P3–O24–Fe2	1	AF	6.92	118	5.82
Fe3–O18–P2–O5–Fe2	1	AF	6.91	115	5.55
Fe3–O14–P5–O2–Fe1	1	AF	6.94	117	5.28
Fe3–O12–P4–O27–Fe1	1	AF	6.95	118	5.36
Average			6.93	118	5.60

109°, due to the existence of P–O–P bonds, and this weakens the interactions (28).

Each iron atom is connected to six surrounding iron atoms through six Fe–O–P–O–Fe links which are antiferromagnetic. The lengths of these pathways and the angles around P (Table 6) are slightly different, leading probably to discriminate between the values of the internal magnetic hyperfine field.

If we consider that the superexchange interaction determines the long-range order, and calling this interaction J, we can estimate its value from the equation investigated by Goodenough (29),

$$T_N = -2J(S+1)S\,n/3\,k = 10\text{ K},$$

where $S = 2.5$ and n is the number of such interactions per iron atom (here, $n = 6$); hence, we obtain $J = -2.5\ 10^{-5}$ meV $= -0.20\text{ cm}^{-1}$, which may be compared with $J = -0.37\text{ cm}^{-1}$ ($T_N = 29$ K) in $NaFeP_2O_7$ (23) and -0.36 cm^{-1} ($T_N = 18$ K) in $Fe_3(P_2O_7)_2$ (30).

CONCLUSION

The C–$Fe(PO_3)_3$ structure is refined using X-ray single-crystal data. In the [010] direction, a subcell structure is present with a period $b/3$, as generally found in other C-form long-chain polyphosphates. The three distinct FeO_6 octahedra, observed through the crystallographic refinement, are also pointed out through Mössbauer spectrometry. In this compound, the magnetic interactions arise from the antiferromagnetic Fe–O–P–O–Fe superexchange mechanism, only.

ACKNOWLEDGMENTS

Neutron diffraction data were recorded at the Institut Laue Langevin (ILL). We are grateful to B. Ouladdiaf, responsible for the spectrometer used, for his help during the measurements.

REFERENCES

1. P. Hautefeuille, *C.R. Acad. Sci.* **96,** 1142 (1883).
2. F. D'Yvoire, *Bull. Soc. Chim. Fr.*, 1237 (1962).
3. A. Durif, "Crystal Chemistry of Condensed Phosphates." Plenum, New York, 1995.
4. H. Van der Meer, *Acta Crystallogr. B* **32,** 2423 (1976).
5. N. Middlemiss, F. Hawthorne, and C. Calvo, *Can. J. Chem.* **55,** 1673 (1977).
6. A. I. Domanskii, Yu. F. Shepelev, Yu. I. Smolin, and B. N. Litvin, *Sov. Phys. Crystallogr.* (*Engl. Transl.*) **27,** 229 (1982).
7. J. Bentama, J. Durand, and L. Cot, *Z. Anorg. Allg. Chem.* **556,** 227 (1988).
8. W. T. A. Harrison, T. E. Gier, and G. D. Stucky, *Acta Crystallogr. C* **50,** 1643 (1994).
9. I. M. Waston, M.M. Borel, J. Chardon, and A. Leclaire, *J. Solid State Chem.* **111,** 253 (1994).
10. P. Rittner and R. Glaum, *Z. Kristallogr.* **209,** 162 (1994).
11. M. Gruss and R. Glaum, *Acta Crystallogr. C* **52,** 2647 (1996).
12. A. Kiel, *Phys. Rev. B* **12,** 1868 (1975).
13. C. Gleitzer, *Eur. J. Solid Inorg. Chem.* **28,** 77 (1991).
14. L. K. Elbouaanani, B. Malaman, and R. Gérardin, *J. Solid State Chem.* **147,** 565 (1999).
15. J. Rodriguez-Carvajal, *Physica B* **192,** 55 (1993).
16. G. Le Caer, private communication.
17. J. A. Ibers and W. C. Hamilton, "International Tables for X-Ray Crystallography," Vol. 4. Kynoch, Birmingham, 1976.
18. G. Sheldricks, Shelx 76, Program for Crystal Structure Determination, Univ. Cambridge, 1976.
19. T. Moya-Pizarro, Roger Salmon, L. Fournes, G. Le Flem, B. Wanklyn, and P. Hagenmuller, *J. Solid State Chem.* **53,** 387 (1984).
20. P. D. Battle, A. K. Cheetham, W. T. A. Harrison, and G. J. Long, *J. Solid State Chem.* **62,** 16 (1986).
21. D. Corbridge, *Bull. Soc. Fr. Mineral Crist.* **94,** 271 (1971).
22. F. Menil, *J. Phys. Chem. Solids* **46,** 763 (1985).
23. L. Terminiello and R. C. Mercader, *Hyper. Interactions* **50,** 651 (1989).
24. D. Beltran-Porter, R. Olazcuaga, L. Fournes, F. Menil, and G. Le Flem, *Rev. Phys. Appl.* **15,** 1115 (1980).
25. I. D. Brown and D. Altermatt, *Acta Crystallogr.* **B41,** 244 (1985).
26. S. V. Karyagin, *Sov. Phys. Solid State* **8,** 391 (1966).
27. G. Le Caer and J. M. Dubois, *Nuclear Instr. Methods* **157,** 127 (1978).
28. P. W. Anderson, *in* "Magnetism" (G. Rado and H. Suhl, Eds.), Vol. 1. Academic Press, San Diego, 1963.
29. J. B. Goodenough, "Magnetism and the Chemical Bond," Publ. Interscience, 1966.
30. M. Ijjaali, G. Venturini, R. Gerardin, B. Malaman, and C. Gleitzer, *Eur. J. Solid. State. Inorg. Chem.* **28,** 983 (1991).